OPEN ACCESS

University of BRISTOL

Harris, S. J., Karsili, T. N. V., Murdock, D., Oliver, T. A. A., Wenge, A. M., Zaouris, D. K., ... Soep, B. (2015). A Multipronged Comparative Study of the Ultraviolet Photochemistry of 2-, 3-, and 4-Chlorophenol in the Gas Phase. The Journal of Physical Chemistry A, 119(23), 6045-56. 10.1021/jp511879k

Peer reviewed version

Link to published version (if available):
10.1021/jp511879k

Link to publication record in Explore Bristol Research
PDF-document

University of Bristol - Explore Bristol Research

General rights

A Multi-Pronged Comparative Study of the Ultraviolet Photochemistry of 2-, 3- and 4-Chlorophenol in the Gas Phase

S.J. Harris, T.N.V. Karsili, D. Murdock, T.A.A. Oliver, [#] A.M. Wenge, [##] D.K. Zaouris, [###]
M.N.R. Ashfold and J.N. Harvey,
School of Chemistry, University of Bristol, BS8 1TS, U.K.

J.D. Few, S. Gowrie and G. Hancock,
Department of Chemistry, Physical and Theoretical Chemistry Laboratory,
Oxford University, South Parks Road, Oxford OX1 3QZ, U.K.

D.J. Hadden, G.M. Roberts and V.G. Stavros,
Department of Chemistry, University of Warwick, Coventry CV4 7AL, U.K.

G. Spighi, L. Poisson and B. Soep,
CNRS, IRAMIS, SPAM, Laboratoire Francis Perrin, URA 2453, F-91191 Gif-sur-Yvette,
France.

No. of Tables: 1
No. of figures: 10

 Current addresses:

[#] Department of Chemistry, University of California, Berkeley, CA 94720-1460, USA.

[##] Carl Zeiss SMT GmbH, Rudolf-Eber-Straße 2, 73447 Oberkochen, Germany.

[###] Institute of Electronic Structure and Laser (IESL), Foundation for Research and Technology - Hellas (FORTH), P.O. Box 1527, GR-71110 Heraklion, Greece.

Abstract

The $S_1(^1\pi\pi^*)$ state of the (dominant) *syn*-conformer of 2-chlorophenol (2-ClPhOH) in the gas phase has a sub-picosecond lifetime, whereas the corresponding S_1 states of 3- and 4-ClPhOH have lifetimes that are, respectively, ~2 and ~3-orders of magnitude longer. A range of experimental techniques – electronic spectroscopy, ultrafast time-resolved photoion and photoelectron spectroscopies, H Rydberg atom photofragment translational spectroscopy, velocity map imaging and time-resolved Fourier transform infrared emission spectroscopy – as well as electronic structure calculations (of key regions of the multidimensional ground (S_0) state potential energy surface (PES) and selected cuts through the first few excited singlet PESs) have been used in the quest to explain these striking differences in excited state lifetime. The intramolecular O–H --- Cl hydrogen bond specific to *syn*-2-ClPhOH is key. It encourages partial charge transfer and preferential stabilisation of the diabatic $^1\pi\sigma^*$ potential (relative to that of the $^1\pi\pi^*$ state) upon stretching the C–Cl bond, with the result that initial C–Cl bond extension on the adiabatic S_1 PES offers an essentially barrierless internal conversion pathway via regions of conical intersection with the S_0 PES. Intramolecular hydrogen bonding is thus seen to facilitate the type of heterolytic dissociation more typically encountered in solution studies.

1. Introduction

The past decade has witnessed giant strides in our understanding of the primary photochemistry of gas phase phenols.[1,2] These systems provide classic examples of dissociation by O–H bond fission on an excited $^1\pi\sigma^*$ potential energy surface (PES), as predicted by Sobolewski *et al*.[3] The ground (S_0) state of phenol correlates diabatically with the excited ($\tilde{A}$) electronic state of the phenoxyl radical. The first excited $^1\pi\pi^*$ state (traditionally labelled S_1) and its triplet $^3\pi\pi^*$ counterpart are bound with respect to R_{O-H}, but the diabatic $^1\pi\sigma^*$ (henceforth S_2) state and the corresponding $^3\pi\sigma^*$ state are both repulsive upon extending R_{O-H} and correlate with ground ($\tilde{X}$) state phenoxyl radical products. The S_2 PES thus exhibits conical intersections (CIs) with the S_1 state (at $R_{O-H} \sim 1.2$ Å) and with the S_0 PES at longer R_{O-H} (~ 2.1 Å).[4] O–H bond fission on the S_2 PES is observed following ultraviolet (UV) excitation of phenol at its S_1–S_0 origin. Most of the energy in excess of that required to break the O–H bond is released as product translational energy. The phenoxyl($\tilde{X}$) products are formed rotationally 'cold' and in a limited sub-set of vibrational (v) states. Systematic studies of the dissociation rates and product vibrational energy disposals following excitation to the S_1 state of phenol and a range of substituted phenols confirm that dissociation involves tunnelling under the S_1/S_2 CI [5] in the O–H stretch coordinate and that this process is facilitated by the $\nu_{16a}(a_2)$ ring puckering and/or OH torsion mode, depending on the molecular symmetry.[4,6,7] Excitation at shorter wavelengths within the S_1–S_0 absorption system populates higher $S_1(v)$ levels. This vibrational excitation tends to be in Franck-Condon active parent modes that are orthogonal to the dissociation coordinate; such excitation contributes relatively little to the tunnelling process and tends to map through into product vibration. Excitation at yet shorter wavelengths, corresponding to energies above the S_1/S_2 CI (typically ~ 240 nm or shorter) allows direct access to the S_2 PES, prompt O–H bond fission and release of H atoms with much higher translational energy.

O–H bond fission is just one of a number of dissociation routes possible on energetic grounds following UV excitation of phenols, however. Most photodissociation experiments focus on a particular product (*e.g.* H atom formation), though a combined experimental (time-resolved Fourier transform infrared (FTIR) emission spectroscopy) and *ab initio* theoretical study of alternative fragmentation pathways following 248 nm and 193 nm excitation of phenol and subsequent radiationless transfer to the S_0 PES is a notable exception.[8]

Such complexity can be expected to increase upon extending to substituted phenols, as illustrated in the present work for the case of chlorophenols (henceforth ClPhOH). These systems offer the possibility of additional dissociation pathways (*e.g.* C–Cl versus O–H bond fission, and possible HCl elimination) from excited states and/or on the ground state PES, at least some of which can be expected to display isomer specificity. 2- and 3-ClPhOH also both exist as *syn-* and *anti*-rotamers (often also termed *cis-* and *trans-*), reflecting the relative orientation of the O–H bond to the Cl atom. In the case of 2-ClPhOH, the *syn*-rotamer is significantly stabilised by the intramolecular hydrogen bond between the hydroxyl H atom and the adjacent Cl atom. Reference 13 summarises various prior studies indicating that this rotamer is ~570 cm^{-1} more stable than the *anti*-rotamer. Jet-cooled S_1–S_0 spectra have been reported for all three isomers.[9–16] Each displays structure, but these studies already point to dramatic isomer-specific variations in S_1 state lifetimes (1.0±0.3 ns for 4-ClPhOH,[17] *cf.* estimates of τ ~0.3 ps in the case of *syn*-2-ClPhOH [13]).

Unsurprisingly, given their toxicity and ubiquity in aquatic systems, the aqueous phase photochemistry of chlorophenols has received much attention, and many such studies have proposed dominant roles for homolytic and/or heterolytic Cl–PhOH bond fission processes under such conditions.[18] Akai *et al* [19] have also compared the IR spectrum of 2-ClPhOH (and various di- and trichlorophenols) in an Ar matrix, pre- and post-UV irradiation, and deduced the formation of cyclopentadienylidenemethanone (CPYM) along with HCl co-products. Here we report a comprehensive isomer- and, where possible, rotamer-selective study of the near UV photochemistry of chlorophenols in the gas phase, using an arsenal of experimental and theoretical methods including (i) electronic spectroscopy of the respective parent molecules, (ii) time-resolved ultrafast pump-probe imaging studies of the evolving excited state population (monitored via the parent ion and the accompanying photoelectrons), (iii) H Rydberg atom photofragment translational spectroscopy (HRAPTS) to monitor H atom forming channels, (iv) velocity map imaging (VMI) to monitor channels leading to formation of ground (Cl) and spin-orbit excited (Cl*) products, (v) time resolved (TR) FTIR emission spectroscopy to monitor vibrationally excited parent molecules and dissociation products like CPYM, HCl and CO, and (vi) electronic structure methods to calculate (a) cuts through the ground and first excited state PESs along $R_{O–H}$ and $R_{C–Cl}$ and for out-of-plane ring distortion towards a prefulvenic structure, and (b) numerous minima and transition states on the ground state PES. These reveal that the greatly reduced S_1 state lifetime in isolated *syn*-2-ClPhOH molecules is a legacy of the intramolecular H-bond and the much-enhanced rate of internal

conversion (IC) enabled by a (relative) lowering of key portions of the adiabatic S_1 potential upon C–Cl bond extension. The present detailed study adds to the growing literature [20,21] detailing ways in which intramolecular H-bonding can suppress excited state dissociation (by facilitating the competing IC route to the S_0 state) and thus enhance photostability in collisional (*i.e.* condensed phase) environments.

2. Experimental and theoretical methods

2-, 3- and 4-ClPhOH were each sourced from Sigma-Aldrich and used as supplied. Details regarding the experimental procedures used in Bristol,[11,22] Warwick,[23] Oxford [24,25] and Gif-sur-Yvette,[26,27] and of the electronic structure calculations,[7] have been given previously and are not repeated here. Further details unique to the present study are available as electronic supplementary information (ESI).

3. Results and Discussion

3.1 *Excitation spectroscopy*

Room temperature UV absorption spectra of 2-, 3- and 4-ClPhOH and jet-cooled 1+1 resonance enhanced multiphoton ionisation (REMPI) spectra of each isomer in the region of the respective S_1–S_0 origins were confirmed as being similar to those reported previously; [9,28,29] these origins and the respective first ionisation potentials are collected in Table I for future reference. Room temperature UV absorption spectra of 2-ClPhOH (in the gas phase and in solution in cyclohexane) and of 3- and 4-ClPhOH (in cyclohexane solution) are shown in the ESI, while figs. 1(a) and 1(b) show jet-cooled 1+1 REMPI spectra of 2- and 3-ClPhOH, plotted on a common wavelength scale. The spectrum of 2-ClPhOH is dominated by the *syn*-conformer – consistent with its greater relative stability. The energy separation between the *syn*- and *anti*-conformers of 3-ClPhOH(S_0), in contrast, is sufficiently small that each shows with comparable intensity in the 1+1 REMPI spectrum. Figure 1 also serves to illustrate the greater width of the *syn*-2-ClPhOH resonances, consistent with the reported short lifetime of this conformer in its S_1 state.[13] All of the same resonances are evident in the excitation spectra for forming H atom fragments (monitored via 1 (121.6 nm) + 1′ (365.7 nm)

REMPI) though, as shown in the ESI, the relative intensities of the weak *anti*-2-ClPhOH resonances are reduced.

3.2   *Ultrafast pump-probe studies*

The time evolution of the population following photoexcitation of the various isomers was investigated by monitoring both ions and photoelectrons. Figure 2(a) shows the time-evolving parent (2-ClPhOH$^+$) ion yield following excitation of 2-ClPhOH with a femtosecond pump pulse centred on the S_1–S_0 band origin (λ_{pump} = 278 nm, with a ~500 cm^{-1} full width half maximum (FWHM) bandwidth) and subsequent probing with a time delayed femtosecond probe pulse centred at λ_{probe} = 243.1 nm. A biexponential fit to this transient (after deconvolving for the finite pump and probe laser pulse durations, the cross-correlation function for which is described using a 120 fs (FWHM) Gaussian) yields decay time constants of τ_1 = 160 ± 30 fs and τ_2 = 750 ± 100 fs. An analogous study at λ_{pump} = 267 nm returned very similar decay constants. As in earlier experiments of this type,[30] λ_{probe} was chosen to enable REMPI detection of any neutral H atom photo-products formed by the pump laser pulse. No H atom signal was detected on the sub-ps timescale of these measurements at either pump wavelength, but prompt H atom formation was observed following femtosecond laser excitation of 2-ClPhOH at λ_{pump} = 200 nm (see ESI). By way of contrast, fig. 2(b) shows the time-dependent 2-FPhOH$^+$ parent ion signal obtained when exciting 2-fluorophenol (2-FPhOH, predominantly if not exclusively its *syn*-conformer) at its S_1–S_0 origin (λ_{pump} = 272 nm) and ionising at λ_{probe} = 243.1 nm. This study returns a 2-FPhOH(S_1) lifetime τ = 2.3±0.2 ns, in reasonable accord with previous estimates from high resolution linewidth studies of the *syn*-conformer (τ = 4.6±0.2 ns and 2.8±0.2 ns [31]) and similar to that found when exciting bare phenol at its S_1–S_0 origin.[5,30] As with phenol, the 2-FPhOH(S_1) decay time constant was seen to decrease on tuning to shorter excitation wavelengths (*e.g.* τ = 1.5 ± 0.1 ns at λ_{pump} = 263 nm).[30]

The temporal decay of the various chlorophenol isomers following excitation to their respective S_1 states was also investigated by time resolved, 266 nm pump, 800 nm (multiphoton) probe photoelectron imaging (TRPEI) methods. Sample images are shown in the ESI. The use of a common pump wavelength necessarily results in population of different S_1(v) levels in each isomer (given the isomer dependent variations in the energy of the S_1–S_0 origin), but the effects of such small variations in internal energy must be small

compared with the huge variations in S_1 lifetime revealed by the TRPEI data shown in figs. 3(a)–3(c). Energetic considerations dictate that a minimum of three 800 nm (1.55 eV) photons are required to ionise these chlorophenol(S_1) molecules (see Table 1), and the measured photoelectron images (such as that shown for 2-ClPhOH in fig. 3(a)) and the electron kinetic energy distributions derived from such images (see ESI) clearly show a major contribution from 4-photon ionisation. The photoelectrons formed by 3-photon ionisation of 2-ClPhOH necessarily have low kinetic energy (E_{el} ~0.1 eV or less); they also show lower recoil anisotropy than the more energetic electrons from 4-photon ionisation. The latter yield is attributed to excitation via super-excited valence states, with the final photon ionising a manifold of Rydberg states, as reported previously for the case of bare phenol.[32] The fingerprint of these Rydberg states (starting from the $4s$ state with an assumed quantum defect $\delta = 1.05$) is evident in the image included within fig. 3(a) and is shown in greater detail in the ESI.

The various photoelectron bands for 2-ClPhOH all show a similar biexponential time decay, characterised by $\tau_1 = 190 \pm 30$ fs and $\tau_2 = 700 \pm 100$ fs, but with very different pre-exponential factors A_i ($i = 1, 2$). A_2 declines continuously from ~0.3 to 0 (relative to $A_1 = 1$) as E_{el} increases to 1.5 eV. The two time constants are in excellent agreement with those determined from the ultrafast pump-probe measurements of the parent ion yield (above). Energetic and Franck-Condon considerations imply that the less energetic electrons formed via 4-photon ionisation must arise from regions of lower potential energy (*i.e.* higher vibrational energy) – lower, in fact, than the S_1 origin, so the finding that the lower energy electrons show a longer (overall) time constant suggests that the $\tau_2 = 700$ fs decay reflects the final crossing to the S_0 state.

We return to this topic, and the role of the intramolecular H bond in facilitating this radiationless transfer in 2-ClPhOH, in section 3.8. The decay time constants determined for the S_1 states of 3-ClPhOH (fig. 3(b)) and 4-ClPhOH (fig. 3(c)) are ~72 ps and ~370 ps, respectively. The latter value agrees reasonably well with that ($\tau = 1.0 \pm 0.3$ ns) estimated from the widths of individual lines in the S_1–S_0 origin band.[17] The TRPEI data for 4-ClPhOH (fig. 3(c)) also shows an interesting E_{el}-dependent early time behaviour, with the high/(low) E_{el} signal showing a decay/(growth) time constant τ ~800 fs. Given that 267 nm photon absorption prepares 4-ClPhOH(S_1) molecules with excess (~1500 cm^{-1}) vibrational energy, we assign this short time evolution to vibrational energy redistribution within the S_1 state.

The TRPEI signals for each isomer decline essentially to zero within the accessible time delays, suggesting that the respective S_1 states decay to the ground (rather than a long lived triplet) state.

3.3   *Time-of-flight measurements of H atom products*

HRAPTS studies of the near UV photolysis of 4-ClPhOH at many different wavelengths have been reported previously.[11] Total kinetic energy release (TKER) spectra derived from time-of-flight (TOF) measurements of the H atom photofragments (together with the assumption that the partner fragment has chemical formula ClC_6H_4O and a mass $m = 127.55$ u) following excitation on the respective S_1–S_0 origin transitions of the *syn*-isomers of 3-and 2-ClPhOH are shown in figs. 4(a) and 4(b). The former displays several peaks attributable to population of specific vibrational levels of the 3-ClPhO radical in its ground electronic state. The individual peak assignments match closely with those reported recently for the 3-FPhO products formed following excitation to the S_1(v=0) level of 3-FPhOH and, as in that case, can be attributed to tunnelling under the S_1/S_2 CI facilitated by parent OH torsional motion.[7] As for PhOH, 3-FPhOH, *etc*, measurements with the electric vector (ε) of the photolysis laser radiation aligned at different angles (θ) to the TOF axis reveal no measurable recoil anisotropy for these H atom fragments. Similarly structured TKER spectra are observed when exciting higher energy resonances within the S_1–S_0 manifold, as shown in the ESI. In contrast, excitation on the S_1–S_0 origin band of *syn*-2-ClPhOH (or any of the other resonances evident in fig. 1(a)) yields TKER spectra that peak at low TKER and are devoid of any fine structure, as illustrated by fig. 4(b). Featureless TKER spectra similar to this have been reported previously, *e.g.* from TOF measurements of the D atom products from photolysis of fully deuterated phenol,[2] and are typically assigned to products of dissociation of vibrationally 'hot' parent molecules after IC to the ground state and/or (in the case of long lived S_1 states) to dissociation following unintended multiphoton excitations.

TKER spectra derived from H atom TOF data from photolysis of both 3- and 2-ClPhOH at much shorter wavelengths (below ~230 nm) show weakly structured features centred at much higher TKER – as illustrated for the specific case of $\lambda = 225$ nm in figs. 4(c) and 4(d). Both show measurable recoil anisotropy. In the case of 3-ClPhOH, the signal is greater when $\theta = 0°$ (*i.e.* recoil anisotropy parameter, $\beta > 0$, implying that these H atom products recoil preferentially parallel to the parent transition dipole moment) whereas, as in PhOH, the H atom signal from short wavelength photolysis of 2-ClPhOH is relatively larger when $\theta = 90°$

(*i.e.* preferential perpendicular recoil, $\beta < 0$). Given the different relative stabilities of the *syn*- and *anti*- conformers of 2-ClPhOH, it is reasonable to assume that the signal in fig. 4(d) is largely from photodissociation of the *syn*-conformer, while the energy splitting of the ground state *syn*- and *anti*-conformers of 3-ClPhOH is presumably too small to significantly degrade the resolution of fig. 4(c). These TKER spectra are reminiscent of those obtained when exciting phenol, and 2- or 3-FPhOH [7] at similarly short wavelengths and, as in those cases, the structure may be plausibly assigned to short progressions in radical mode ν_{18b} (an in-plane C–O/C–Cl wagging motion in this case). Since both are asymmetrically substituted phenols, we associate the fastest peak in each TKER spectrum to formation of H atoms in association with the partner radical in its zero-point (v=0) vibrational level. Analysis of TKER spectra of each isomer recorded at many different wavelengths yield the respective bond dissociation energies: $D_0(syn\text{-}2\text{-ClPhO–H}) = 30940\pm50$ cm^{-1} and $D_0(3\text{-ClPhO–H}) = 30500\pm50$ cm^{-1}. Taken together with the previous determination of $D_0(4\text{-ClPhO–H}) = 29520\pm50$ cm^{-1} (ref. 11) these values serve to illustrate (a) the reduction in O–H bond strength caused by introducing an electron rich Cl atom at the 4- rather than 3-position (*i.e.* by stabilising the radical product) and (b) the increase in O–H bond strength in the *syn*-2-conformer (*i.e.* the stabilisation of the S_0 parent molecule by intramolecular H-bonding).

3.4   VMI studies of Cl and Cl* atom products

Imaging chlorine atom products from chlorophenols is complicated by the presence of much larger ion signals at $m/z \geq 36$ which we attribute to $C_3H_n^+$ (n=0-3) fragment ions; indeed, our previous studies of 4-ClPhOH failed to identify any Cl or Cl* products that could be unambiguously attributed to one photon induced dissociation.[22] In the present work, however, we did succeed in obtaining 'one colour' images of Cl and Cl* products from photolysis of 2-ClPhOH at, respectively, 235.33 nm and 235.21 nm – the standard wavelengths for 2+1 REMPI detection of ground (Cl) and spin-orbit excited (Cl*) atoms.[33] As fig. 5 shows, both images are isotropic, though the Cl* signal is substantially weaker, and the distributions derived therefrom both peak at low TKER (~2000 cm^{-1}, calculated on the basis that the partner fragment has chemical formula C_6H_5O and a mass $m = 93.11$ u).

3.5   Time resolved FTIR emission spectroscopy

TR-FTIR methods were used to investigate the emission from vibrationally excited products arising from a room temperature sample of 2-ClPhOH following excitation at three different

wavelengths: 266 nm, 226 nm and 193.3 nm. Figure 6 shows a compilation of FTIR emission spectra (in the form of a false colour plot) recorded over the wavenumber range 2000-3100 cm^{-1} at numerous time delays in the range 0-90 μs following photolysis of 2-ClPhOH at 193.3 nm. Three band systems are clearly evident: (i) an intense emission in the 2000-2150 cm^{-1} range that narrows and blue-shifts with increasing time delay (ending at a centre value of ~2107 cm^{-1}), attributable to the C=C=O asymmetric stretch mode of CPYM; (ii) a more persistent feature in the same wavenumber region, centred at ~2140 cm^{-1} and attributable to $\Delta v = -1$ transitions of CO; and (iii) a richly structured emission in the 2500-3100 cm^{-1} range which can be assigned to vibrationally excited (but collisionally rotationally thermalized) HCl products − the co-fragment accompanying formation of CPYM. Upon deuteration of the hydroxyl group in 2-ClPhOH, emission in the HCl region was markedly reduced, but the expected emission from DCl was obscured by the intense CPYM emission near 2000 cm^{-1}. Qualitatively, at least, this result is consistent with the expectation that HCl elimination involves the hydroxyl H atom rather than an H atom from the ring. Similar emission from rovibrationally excited CO molecules was reported in an earlier TR-FTIR study of phenol photolysis at 193.3 nm,[8] and companion electronic structure calculations for a range of isomerization and dissociation reactions on the PhOH(S$_0$) PES (at the G2M//B3LYP/6-311G(d,p) level of theory) identified CO and H$_2$ eliminations (the latter yielding CPYM as the co-product) as the least endoergic decomposition pathways. The same HCl ($\Delta v = -1$), CO ($\Delta v = -1$) and CPYM emissions were observed when exciting 2-ClPhOH at 226 nm and at 266 nm, though comparison of the HCl contours recorded at early time delays indicates less vibrational excitation in the products formed at the longer excitation wavelengths (see ESI). Figure 7 highlights clear differences between the early time ($\Delta t = 4$ μs) IR emission from 2-ClPhOH following excitation at (a) 226 nm and (b) 266 nm. The latter shows additional features in the 3000-3600 cm^{-1} region which, as fig. 7(c) shows, are consistent with vibrationally excited parent *syn*-2-ClPhOH molecules.[34]

3-ClPhOH was studied less extensively by TR-FTIR emission spectroscopy, and 4-ClPhOH not at all (due to its substantially lower vapour pressure). The appearance and evolution of the feature attributable to CPYM following 193.3 nm photoexcitation of 3-ClPhOH is indistinguishable from that observed when exciting 2-ClPhOH at the same wavelength, but analysis of the HCl emissions suggests that the partner HCl products carry less vibrational excitation than their counterparts from 2-ClPhOH.

3.6   Summary of Experimental Findings

These complementary measurements:

(i)   Confirm (and quantify) the previously recognised [13] sub-ps lifetime of the S_1 state of *syn*-2-ClPhOH. The corresponding excited state lifetimes for 3- and 4-ClPhOH are, respectively, ~2 and ~3-orders of magnitude longer. The S_1 state of 2-FPhOH, in contrast, is found to have a nanosecond lifetime (similar to that of PhOH [30]), while previous absorption studies imply that the lifetime of the S_1 state of *syn*-2-BrPhOH is even shorter than that of *syn*-2-ClPhOH.[13]

(ii)   Reveal prompt O–H bond fission when exciting all three chlorophenol isomers at short wavelengths (*i.e.* at energies above the S_1/S_2 CI). The derived TKER spectra are similar to those obtained when exciting PhOH at such short wavelengths and are consistent with dissociation on the $S_2(^1\pi\sigma^*)$ PES.[2,7] Exciting 3- and 4-ClPhOH at long wavelengths (*i.e.* on S_1–S_0 resonances below the S_1/S_2 CI) yields some translationally excited H atoms attributable to O–H bond fission by tunnelling through the barrier under the S_1/S_2 CI (more clearly in the case of 3-ClPhOH). No corresponding H atom signal was detected when exciting *syn*-2-ClPhOH at these energies, thus eliminating such tunnelling as a possible cause of the much enhanced *syn*-2-ClPhOH(S_1) loss rate.

(iii)   Demonstrate formation of HCl, CO and CPYM following excitation of 2-ClPhOH at 193.3, 226 and 266 nm, as well as vibrationally excited parent molecules at the longest of these wavelengths. Cl (and Cl*) atoms were also detected when exciting at ~235 nm, with isotropic velocity distributions that peak at low TKER. HCl, CO and CPYM products were also identified following 193.3 nm excitation of 3-ClPhOH.

The latter products show obvious parallels with those reported following 193.3 nm photolysis of gas phase PhOH, which have been plausibly interpreted in terms of unimolecular decay of highly vibrationally excited molecules formed following radiationless transfer to the S_0 PES.[8] Analogy with previous studies of chlorobenzene photolysis [35] led Yamamoto *et al*.[13] to suggest intersystem crossing to a $^3\pi\sigma^*$ state (the equilibrium geometry for which involved an extended C–Cl bond length) as the cause of the dramatic reduction in S_1 lifetime in the case

11

of *syn*-2-ClPhOH. Our recent comparative studies of photoinduced halogen (Y) atom loss from the family of 4-YPhOH (Y = I, Br and Cl) molecules, in contrast, identified triplet state participation in the case that Y = I only.[22] In what follows, we thus look again for singlet state only (*i.e.* spin conserving) routes to explain the observed photochemistry of the gas phase chlorophenols. We start by considering the various possible fates of chlorophenol molecules following radiationless transfer to the S_0 PES, then move on to explore various radiationless transfer routes to the S_0 state from higher singlet states.

3.7   Topology of the S_0 PES

The ground state PESs for unimolecular dissociation of 2- and 4-ClPhOH were calculated at the B3LYP/6-31G(d) level of theory (with single-point energy calculations using the larger 6-311+G(*d,p*) basis) in order to rationalize the loss of H_2, CO and HCl fragments. Many of the intermediates and transition states (TSs) are similar or identical to those located in earlier studies of PhOH [8,36] and 2-ClPhOH [37] but, for completeness, all the key stationary points have been located again at a consistent level of theory. Further details of these calculations are given in the ESI. Similar dissociation processes have also been described for unimolecular decay of molecular ions of phenol and related species.[38] The B3LYP density functional theory (DFT) method used here is not quantitative but, within expected error bars of order 5 kcal mol^{-1} (~0.2 eV), should provide a reasonable description of the relative energies of the various dissociation asymptotes and the transition states joining them. Test calculations using single-reference correlated *ab initio* methods (as in ref. 8) suggest that these methods may not be more accurate than B3LYP for the present system due to the significant multi-reference character of some of the TSs.

The B3LYP/6-311+G(*d,p*)//B3LYP/6-31G(*d*) level of theory used here reproduces the features of the PES for PhOH dissociation found in previous studies [8,36] reasonably well. For example, the key TSs leading to loss of H_2 or CO (TSs 1 and 14 in ref. 8) lie, respectively, 98.9 and 81.0 kcal mol^{-1} above the phenol minimum using the present methodology (*cf.* 102.1 and 75.8 kcal mol^{-1} in ref. 8). Note that all quoted energies derived in the present work include a correction for zero-point energy using the B3LYP/6-31G(d) wavenumbers. The calculated energy for H atom loss by O–H bond cleavage is also reproduced quite well (81.6 kcal mol^{-1}, *cf.* 89.1 kcal mol^{-1} in ref. 8).

Apart from the H atoms attributed to tunnelling under the S_1/S_2 CI in the R_{O-H} coordinate 3- and 4-ClPhOH, all of the fragments observed in the long wavelength photolysis of the

chlorophenols are attributed to unimolecular decay of vibrationally excited S_0 molecules formed by radiationless transfer after electronic excitation. Many minima and connecting TSs are accessible at the photon energies used in the present work; only a relevant subset of these pathways is shown in fig. 8. Several bond cleavage processes yielding H or Cl atoms (plus a partner radical) are identified by the present calculations, with O–H bond fission predicted to be the least endoergic (D_0(H–OPhCl) = 83.3 kcal mol^{-1}) though the C–Cl bonds are also predicted to be relatively weak. We also note that the D_0(*syn*-2-ClPhO–H) value determined in the companion experimental studies (88.5 kcal mol^{-1} (section 3.3)) reinforces an earlier conclusion [8] that the methods used in the present calculations are likely to underestimate the O–H bond strengths.

Several molecular elimination processes are also possible and, as fig. 8 shows, the lowest-energy barriers leading to these products in some cases lie below the asymptotes for direct bond cleavage. The variational TSs leading to bond cleavage will be significantly looser than the saddle-point TSs involved in molecular elimination, but the earlier RRKM studies [8] suggest that the molecular elimination pathways will dominate, at least at lower energies. Four molecular fragments can, in principle, be eliminated yielding relatively low-energy fragments: H_2, H_2O, HCl and CO. Loss of H_2 from the phenol OH group and an adjacent C–H bond involves barriers >100 kcal mol^{-1} and is not shown in fig. 8. Loss of H_2O with formation of a benzyne derivative is also calculated to involve a rather high barrier labelled TS **A** in fig. 8. (Note that, in order to avoid overloading fig. 8, this TS is only shown for H_2O loss from 4-ClPhOH, but a similar TS (**A′**) with a very similar barrier exists for H_2O loss from 2-ClPhOH).

The processes with lower energy barriers involve elimination of HCl and of CO. For the former, HCl loss with concerted ring contraction can occur through the (previously identified [37]) TS **B**, to yield a cyclopentadienyl ketene derivative (CPYM) – the calculated energy of which is E = 27.6 kcal mol^{-1} above the S_0 minimum. The structure of TS **B** (calculated at E = 75.2 kcal mol^{-1}) involves a largely broken C–Cl bond ($R_{C–Cl}$ = 3.17 Å *cf.* 1.77 in *syn*-2-ClPhOH(S_0)), with the new C–C bond only partly formed (2.00 Å *vs.* 1.46 Å). The C–O bond length at the TS (1.23 Å) is closer to that in the product ($R_{C–O}$ = 1.16 Å) than in the starting species (1.36 Å). Nonetheless, the difference in C–O bond length at the TS compared to that in CPYM would be sufficient to account for the observed vibrational excitation of the nascent product. Another possible HCl loss route involves the higher-energy TS **C** (at E = 85.3 kcal mol^{-1}) after formation of the cyclohexadienone tautomer of ClPhOH

13

through TS **D**. TS **C** also involves concerted HCl loss and ring contraction, and likewise has a short C–O bond length (R_{C-O} = 1.19 Å). HCl loss from 4-ClPhOH can also occur, since 2- and 4-ClPhOH can interconvert through a variety of relatively low-energy multi-step pathways, one of which is shown in fig. 8. From 2-ClPhOH, H transfer from the OH group to the adjacent Cl-bearing carbon through TS **D** forms a cyclohexadienone species. Two subsequent H-atom shifts (TSs **E** and **F**) followed by one Cl-atom shift (TS **G**) yields an isomeric cyclohexadienone, which can then convert over the barrier associated with TS **H** to 4-ClPhOH. CO elimination involves formation of a bicyclic species from one of the intermediates along this isomerisation pathway, over TS **I**. The bicyclic species can then lose CO through TS **J**. There are several isomers of the bicyclic species, depending on the position of the chlorine substituent, but only one (leading to the lowest-energy form of TS **J**, at E = 81.4 kcal mol^{-1}) is shown in fig. 8.

3-ClPhOH has been considered here in less detail and, for the sake of clarity, the associated energies are not shown in fig. 8. The S_0 minimum is calculated to lie 0.8 kcal mol^{-1} above that of *syn*-2-ClPhOH, and several possible dissociation and isomerisation pathways can be considered. Here, we describe one possible route that could lead ultimately to loss of HCl and formation of the CPYM product. First, 3-ClPhOH can convert to 5-chlorocyclohexadienone (E = 17.2 kcal mol^{-1}) through a TS analogous to TSs **D** and **H** (lying at E = 66.6 kcal mol^{-1}). In turn, this species can isomerize to the 6-chlorocyclohexadienone species shown in fig. 8 (at E = 23.6 kcal mol^{-1}) through a two-step process. First, an H atom shifts from position 6 to 5 through a TS analogous to TS **G** (E = 64.9 kcal mol^{-1}) to form a biradical intermediate lying at E = 57.1 kcal mol^{-1}. The latter then undergoes a 5,6 Cl atom shift through a chloro-analogue of TS **G** (E = 74.5 kcal mol^{-1}), thereby offering one relatively low-energy process enabling interconversion between 2- and 3-ClPhOH.

In summary, these DFT calculations show that the key TSs for loss of HCl or CO from 2-, 3- and 4-ClPhOH all lie well below the longest wavelength photon energies used in the present experiments, and below the asymptotes corresponding to O–H or C–Cl bond cleavage. Suitable isomerisation TSs have also been located at sufficiently low energies to permit rapid interconversion between the isomers prior to dissociation.

3.8   *Radiationless transfer to the S_0 PES*

Figure 9 displays cuts through the PESs of the ground and first excited singlet states of 2- and 4-ClPhOH calculated as functions of three nuclear distortions, with a view to identifying possible differences in the non-radiative decay pathways available to the respective S_1 molecules. The open points in panels (a) and (d) depict cuts along R_{O-H} – arguably the most studied dissociation pathway from the S_1 state of phenol and substituted phenols [4,6] – with all atoms constrained to lie in the plane. O–H bond fission from the S_1 state of either isomer under such circumstances would require the molecule to tunnel under the S_1/S_2 CI. The magnitude of this barrier (relative to the respective S_1(v=0) levels) at C_s geometries is calculated to be very similar in the two isomers. Such a simple O–H bond fission mechanism is thus unlikely to offer an explanation for the orders of magnitude difference in the lifetimes of the S_1 states of 2- and 4-ClPhOH, though we will return later to consider the adiabatic S_1 potentials displayed via filled points in panels (a) and (d).

Panels (b) and (e) compare the energy profiles for another much studied coordinate when considering internal conversion in benzene derivatives – the out-of-plane ring deformation leading to a low energy S_1/S_0 CI with prefulvenic geometry.[39] Starting from the respective S_1 minima, both 2- and 4-ClPhOH molecules would need to surmount ~1 eV potential barriers in order to access this CI. Thus it appears improbable that this radiationless pathway could account for the sub-picosecond lifetime of the 2-ClPhOH(S_1) state.

Panels (c) and (f) explore a third coordinate, the C–Cl stretch. The PECs defined by open points show linear interpolations in internal coordinates (LIICs) between the minima of the diabatic $^1\pi\pi^*$ and $^1\pi\sigma^*_{C-Cl}$ states (and beyond), calculated with all atoms confined to the C_s ring plane. The symmetry constrained adiabatic S_1 PECs for 2- and 4-ClPhOH are broadly similar, with an obvious minimum (from the diabatic $^1\pi\pi^*$ state) at $R_{C-Cl} \sim 1.78$ Å, a barrier (the lower cone of the CI between the diabatic $^1\pi\pi^*$ and $^1\pi\sigma^*_{C-Cl}$ states at $R_{C-Cl} \sim 2.1$ Å) and a shallow minimum (associated with the diabatic $^1\pi\sigma^*_{C-Cl}$ state) at longer R_{C-Cl} (~2.6 Å in the case of 2-ClPhOH (fig. 9(c)). Isomer specific differences become much more evident once C_s symmetry constraints are lifted. The filled points in panels (c) and (f) show the adiabatic S_1 PECs obtained by stepping the C–Cl bond length and, at each R_{C-Cl} value, allowing all other internal degrees of freedom to relax to the minimum energy configuration. Such relaxation has relatively little effect in the case of 4-ClPhOH(S_1) (fig. 9(f)); the minimum energy PEC still presents a ~1 eV barrier to dissociation from the S_1 minimum. The situation

with 2-ClPhOH is very different. The calculated minimum energy path on the relaxed S_1 PEC in this case is now essentially barrierless (fig. 9(c)). This dramatic reduction in barrier height is achieved by the C–Cl bond moving out of the ring plane. The minimum energy pathway involves passage around the $^1\pi\pi^*/^1\pi\sigma^*_{C-Cl}$ CI *via* motion along the C–Cl out-of-plane wagging coordinate. This conclusion is confirmed by inspecting the calculated (harmonic) wavenumbers of the normal mode vibrations of 2-ClPhOH at the (C_s constrained) $S_1(^1\pi\pi^*)$ minimum (listed in the ESI), which return an imaginary value for the C–Cl out-of-plane wagging motion.

Key to understanding the very different topologies of the adiabatic S_1 potentials for 2- and 4-ClPhOH is the nature of the diabatic $^1\pi\sigma^*_{C-Cl}$ state. The σ^* orbital is delocalized over the C and Cl atoms in the vertical Franck Condon (vFC) region but can acquire dominant C or Cl character upon stretching R_{C-Cl}. The corresponding σ orbital will relax in the opposite direction, gaining dominant Cl or C character. These two orbitals contain a total of three electrons in the diabatic $^1\pi\sigma^*_{C-Cl}$ state. In the case of 4-ClPhOH, increasing R_{C-Cl} will lead to a progressive localisation of the σ^* orbital on Cl, so the σ electrons can be pictured in an sp^2 orbital on carbon atom 4. This is favoured because the state then has overall 4-PhOH* ---- Cl character (*i.e.* a Cl atom and an excited state of the 4-PhOH radical, in which an electron has moved from the π system into the sp^2 hybrid orbital on the carbon atom at the 4-position). Both fragments are neutral. In the case of 2-ClPhOH, the same type of configuration will dominate at very large R_{C-Cl} but, at intermediate distances, the presence of the intramolecular O–H --- Cl hydrogen bond will stabilize the other resonance form, with 2-PhOH$^+$ ---- Cl$^-$ character, in which the σ^* orbital is largely on carbon atom 2 and the σ electrons are on Cl. Formally, this leads to a negative charge on chlorine, and the phenolyl fragment has a positive charge. The hydrogen bond in this resonance form is very strong (due to the presence of a cationic H-bond donor and an anionic chlorine acceptor). This is enough to counteract the preference for a neutral state, and has the effect of lowering the energy of the $^1\pi\sigma^*_{C-Cl}$ state at intermediate values of R_{C-Cl} (relative to that in 4-ClPhOH). The $^1\pi\pi^*$ state, in contrast, is not strongly affected by the 2- or 4-substitution, so the relative stabilisation of the $^1\pi\sigma^*_{C-Cl}$ state in 2-ClPhOH lowers the energy at which it crosses the $^1\pi\pi^*$ state and thus leads to the behaviour described.

We now return to consider the filled points in panels (c) and (a), which show the adiabatic S_1 PECs obtained by progressively extending the O–H bond length and, at each R_{O-H}, allowing

all other internal degrees of freedom to relax to the minimum energy geometry. The parallels with the adiabatic PECs shown in panels (c) and (f) are both obvious, and reassuring. Again, the effect of such geometry relaxation has little effect on the adiabatic PEC for the S_1 state of 4-ClPhOH, whereas the minimum energy path on the fully relaxed 2-ClPhOH(S_1) potential is essentially barrierless – as a result of the previously identified relocation of the Cl atom.

Notwithstanding the likely uncertainties associated with the energies reported in fig. 8, it is improbable that the C–Cl bond strength exceeds the energy of the S_1(v=0) level. Nonetheless, no fast Cl (or H) atoms were detected when 2-ClPhH is excited near its S_1 origin. Thus we still need to identify a radiationless decay pathway for 2-ClPhOH molecules to the S_0 state that is facilitated by C–Cl bond extension. This we have not explored exhaustively, but fig. 10 shows the geometry of one low energy CI between the adiabatic S_1 and S_0 PESs, identified (using Gaussian 09 and the CASSCF(10,8)/3-21G level of theory) at $R_{C–Cl}$ ~4.01 Å, which can be accessed from the long range minimum on the adiabatic S_1 PES, is well posed to release HCl and is somewhat reminiscent of the structure at TS **B** in fig. 8.

3.9   *Summary discussion*

Theory thus provides a rationale for the dramatically reduced lifetime of *syn*-2-ClPhOH(S_1) molecules (*cf.* that for 3- or 4-ClPhOH(S_1) molecules). The relative stability of the *syn*- and *anti*-conformers of 2-ClPhOH means that the population of the latter is too low to study in the present experiments, but the foregoing interpretation implies that *anti*-2-ClPhOH(S_1) molecules should display a nanosecond lifetime. Reverting to *syn*-2-ClPhOH, we might speculate that the observed biexponential decay revealed by the ultrafast pump-probe studies (section 3.2) may provide some measure of the timescales for S_1 population to evolve from the vFC region to the shallow minimum at extended $R_{C–Cl}$, followed by eventual relaxation to the S_0 ground state. The reality may be less straightforward however, if the diabatic S_1 and S_2 states are sufficiently mixed in the vFC region that femtosecond excitation prepares a range of states with mixed $\pi\pi^*/\pi\sigma^*$ character. Such mixing might account for the obvious asymmetry of the lifetime broadened peaks in the 1+1 REMPI spectrum of 2-ClPhOH (fig. 1(a)), though any attempt at validating this suggestion must be complicated by the predicted double minimum (in the C–Cl out-of-plane wag coordinate) in the S_1 potential.

Extrapolating this theory also offers a rationale for the very different decay rates of S_1 state 2-FPhOH and 2-BrPhOH molecules. The carbon−halogen bond in 2-BrPhOH is weaker than in

2-ClPhOH, so it is reasonable to expect that radiationless transfer to the S_0 state via initial carbon–halogen bond extension will be at least as effective as in the case of 2-ClPhOH – consistent with the experimentally derived sub-ps lifetime of the 2-BrPhOH(S_1) state.[13] (As in chlorophenol, the 4-BrPhOH(S_1) state has a much longer lifetime – as demonstrated by the well resolved vibronic structure in the corresponding 1+1 REMPI spectrum.[11]) The S_1 state of 2-FPhOH, in contrast, has a nanosecond lifetime (recall fig. 2(b)). This, too, is understandable in light of the foregoing theory. The much greater strength of the C–F bond will elevate the $^1\pi\sigma^*_{C\text{-}F}$ potential relative to the $^1\pi\pi^*$ minimum, thereby ensuring that the $^1\pi\pi^*/^1\pi\sigma_{C\text{-}F}^*$ CI constitutes a barrier to C–F bond extension and closing the possible IC route facilitated by such motion. Consistent with the foregoing, we also note that high resolution spectroscopy studies of 2-FPhOH (*syn*-conformer) concluded that the S_1 state had a double minimum potential (but were not able to identify the relevant out-of-plane coordinate).[31] It seems unlikely that intramolecular H-bond assisted IC should be restricted solely to the heavier halophenols, and future studies might logically search for similar effects in, for example, 2-halosubstituted thiophenols and anilines.

Finally we consider whether the available data offers insights into the relative quantum yields of the various possible decay channels in these and related phenols, and their variation with excitation energy. The various fluorophenols all have similar reported S_1 state lifetimes: *syn*-2-FPhOH, $\tau = 2.3\pm0.2$ ns, fig. 2(b)); *syn*- and *anti*-3-FPhOH, $\tau = 1.9\pm0.1$ and 2.7 ± 0.2 ns, respectively;[5] 4-FPhOH, $\tau = 1.7\pm0.1$ ns.[5] The reported lifetime for 4-FPhOD(S_1) molecules is not much longer: $\tau = 3.2$ ns.[40] The reported lifetimes for PhOH(S_1) and PhOD(S_1) molecules are also similar: 2.2 ns and 13.3 ns, respectively.[41] Tunnelling estimates for a range of phenols suggest that deuterating the O–H bond should result in a ~1000-fold reduction in the barrier penetration rate.[6] Thus the available experimental data reinforces the expectation that tunnelling under the S_1/S_2 CI makes negligible contribution to the decay of S_1 state PhOD (and FPhOD) molecules, but that the rate of this tunnelling process is competitive with that for fluorescence and other (slow) IC pathways in the fully hydrogenated analogues.

The calculated 1-D barriers to O–H bond fission under the S_1/S_2 CI in the $R_{O\text{–}H}$ stretch coordinate in 2- and 4-ClPhOH are of similar magnitude, implying a tunnelling rate constant ~10^8 s^{-1} (*cf.* the >10^{12} s^{-1} total loss rate constant measured for *syn*-2-ClPhOH(S_1) molecules). Clearly, the C–Cl stretch mediated IC mechanism identified in the present work is the dominant decay pathway, and the various product yields will be determined by the respective

unimolecular decay rate constants of the resulting highly vibrationally excited parent S_0 molecules at the excitation energy of interest. These have not been estimated in the present work, but we can anticipate their relative rates (and their variation with excitation energy) by reference to the earlier study of phenol photolysis.[8] As in that study, fig. 8 identifies CO elimination (via TSs **D**, **E**, **F**, **I** and **J**) as a low energy channel, supplemented in the present case by a rival HCl elimination channel (via TS **B**). Guided by the earlier unimolecular rate constant estimates,[8] we conclude that both should be major channels when exciting at long wavelengths (consistent with the present observations of CO, HCl (and its partner product CPYM) in the TR-FTIR studies at 266 nm), but that the alternative O–H bond fission on the S_0 PES must become increasingly important as the excitation wavelength is reduced. C–Cl bond extension is identified as the key motion enabling rapid IC following excitation to the S_1 state of *syn*-2-ClPhOH, but no Cl atom products are observed at these long wavelengths and the respective dissociation energies (fig. 9) and masses suggest that C–Cl bond fission will never be a serious competitor to O–H bond fission on the S_0 PES − consistent with our inability to detect anything other than a weak one colour Cl atom image when exciting at 235 nm. The HRAPTS studies reveal a further (excited state) contribution to the H atom yield following excitation of all three chlorophenols at energies above the S_1/S_2 CI in the O–H stretch coordinate, but the persistence of CO, HCl and CPYM emissions when exciting *syn*-2-ClPhOH at 226 nm and both *syn*-2-ClPhOH and 3-ClPhOH at 193.3 nm indicates that competitive IC routes to the S_0 PES persist at much higher excitation energies.

Associated content

Additional experimental details relating to the time resolved FTIR emission studies; further details regarding the computational methods employed; UV absorption spectra of 2-, 3- and 4-chlorophenol; comparisons between the 1+1 REMPI and H atom PHOFEX spectra of 2- and 3-ClPhOH when exciting near the respective S_1–S_0 origins; time resolved H^+ fragment and parent ion yield data following 200 nm excitation of 2-ClPhOH; selected time resolved photoelectron images following 266 nm excitation of 2-ClPhOH and their analysis; TKER spectra derived from H atom PTS measurements at several different wavelengths near the S_1–S_0 origins of 2- and 3-ClPhOH; HCl product vibrational distributions deduced from analysis of FTIR emission spectra following 2-ClPhOH photolysis at 266, 226 and 193 nm; calculated harmonic wavenumbers of the normal mode vibrations of 2-ClPhOH at the C_s constrained

minimum energy geometry of the $S_1(^1\pi\pi^*)$. This material is available free of charge *via* the Internet at http://pubs.acs.org.

Corresponding author:

mike.ashfold@bris.ac.uk; tel. +44(0)1179288312

Notes

The authors declare no competing financial interest.

Table I

S$_1$–S$_0$ band origins and adiabatic first ionisation potentials of 2-, 3- and 4-chlorophenol.

	S$_1$–S$_0$ origin / cm^{-1} [ref.]	I.P.$_{(adiab)}$ / eV [ref.]
2-ClPhOH, *syn*	35892 [13]	~8.9 [29]
2-ClPhOH, *anti*	35702 [13]	
3-ClPhOH, *syn*	35769 [15]	8.65 [15]
3-ClPhOH, *anti*	35889 [15]	8.68 [15]
4-ClPhOH	34811 [11]	8.44 [10]

Figure Captions

Figure 1

Jet-cooled 1+1 REMPI spectra of (a) 2-ClPhOH and (b) 3-ClPhOH, with peak assignments from refs. [13], [15] and [16].

Figure 2

Parent ion transient signals for (a) 2-ClPhOH and (b) 2-FPhOH following femtosecond pulsed laser excitation at their respective S_1–S_0 band origins and time-delayed ionisation with a second femtosecond pulse at 243.1 nm.

Figure 3

Photoelectron transients for (a) 2-, (b) 3- and (c) 4-ClPhOH following femtosecond excitation at 266 nm and time-delayed ionisation by absorption of multiple 800 nm photons. The false colour plot in (a) shows the velocity (vertical axis) dependent yields and temporal decay behaviour (horizontal axis). The two traces in (a) highlight the differing time dependence of two (arrowed) components within the photoelectron yield with E_{el} = 0.15 and 0.45 eV. The two traces in (c) illustrate the different time dependences of high E_{el} (defined by a Gaussian centred at E_{el} = 0.44 eV with 0.14 eV FWHM, and shown in red) and low E_{el} (Gaussian centred at E_{el} = 0.27 eV with 0.09 eV FWHM, shown in blue) parts of the photoelectron yield.

Figure 4

TKER spectra derived from H atom TOF spectra recorded following nanosecond pulsed laser excitation of (a) *syn*-3-ClPhOH and (b) *syn*-2-ClPhOH at the respective S_1–S_0 band origins. TKER spectra obtained from H atom TOF spectra measured following excitation of 3- and 2-ClPhOH at 225 nm are shown in (c) and (d), respectively.

Figure 5

TKER distributions derived from one colour VMI images of the Cl and Cl* atoms (shown in the insets) following excitation of 2-ClPhOH at (a) 235.33 nm and (b) 235.21 nm. The photolysis laser in each case was polarised vertically in the plane of the image (as shown by the double headed arrows).

Figure 6

False colour plot showing IR emission spectra (in the range 2000-3100 cm^{-1}) recorded as a function of time delay (over the range $0 < \Delta t < 90$ μs) following 193.3 nm photolysis of a 20 mTorr sample of 2-ClPhOH.

Figure 7

IR emission spectra in the range 2500-3800 cm^{-1} recorded at $\Delta t = 4$ μs following excitation of a 20 mTorr sample of 2-ClPhOH at (a) 226 nm (5 cm^{-1} resolution) and (b) 266 nm (20 cm^{-1} resolution). Trace (c) depicts the relevant region of the 2-ClPhOH absorption spectrum.

Figure 8

Schematic computed (B3LYP/6-311+G(d,p)//B3LYP/6-31G(d)) PES for isomerisation and dissociation of ClPhOH(S$_0$) molecules. The horizontal red line indicates the (experimental) energy of the S$_1$(v=0) level. (To aid comparison with ref. [8], all energies are reported in kcal mol^{-1}, but can readily be converted to eV using the equivalence 1 eV = 23.06 kcal mol^{-1}).
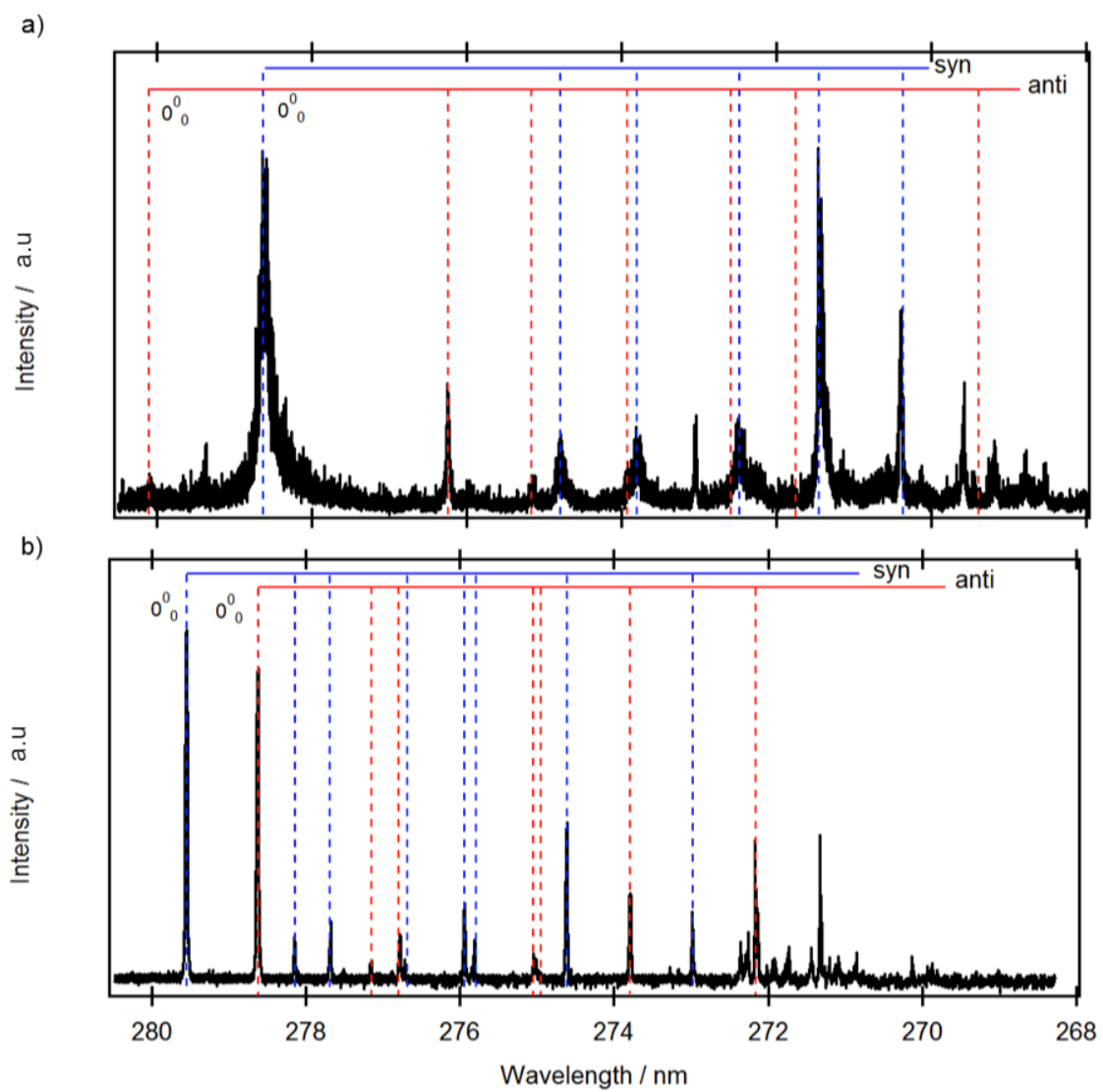
Figure 9

Cuts through the ground and first excited singlet PESs of 2-ClPhOH ((a)–(c)) and 4-ClPhOH ((d)–(f)) plotted as functions of R_{O-H} ((a) and (d)), out-of-plane deformation ((b) and (e)) and R_{C-Cl} ((c) and (f)). The excited state PECs in panels (a), (c), (d) and (f) are shown with (open points) and without (filled points) the constraint of C_s symmetry with, in the latter cases, the calculated S$_1$ minimum energy geometries depicted at selected R_{O-H} / R_{C-Cl} bond extensions.

Figure 10

Geometry of a low energy CI identified between the adiabatic S$_1$ and S$_0$ states of 2-ClPhOH at R_{C-Cl} ~4.01 Å.
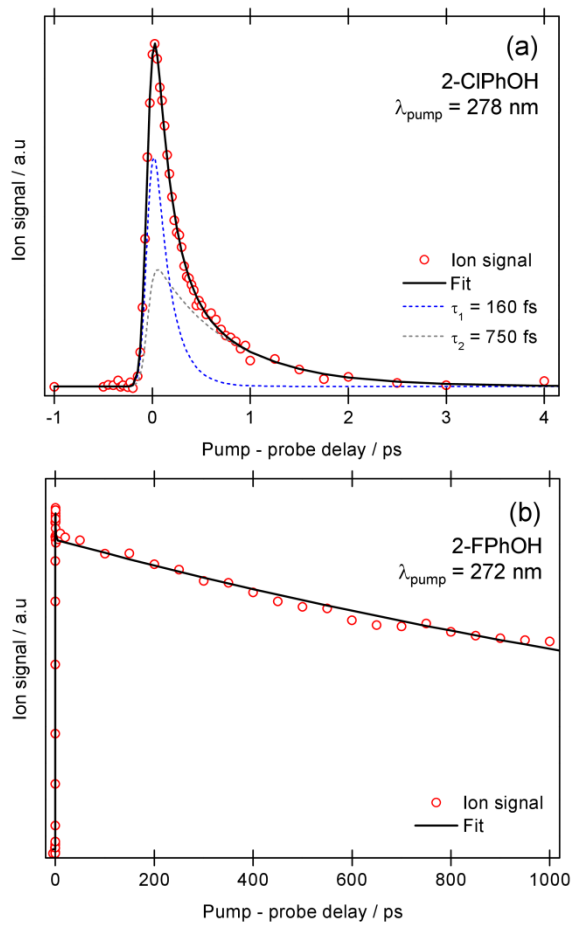
Figure 1

Figure 2

Figure 3

Figure 4
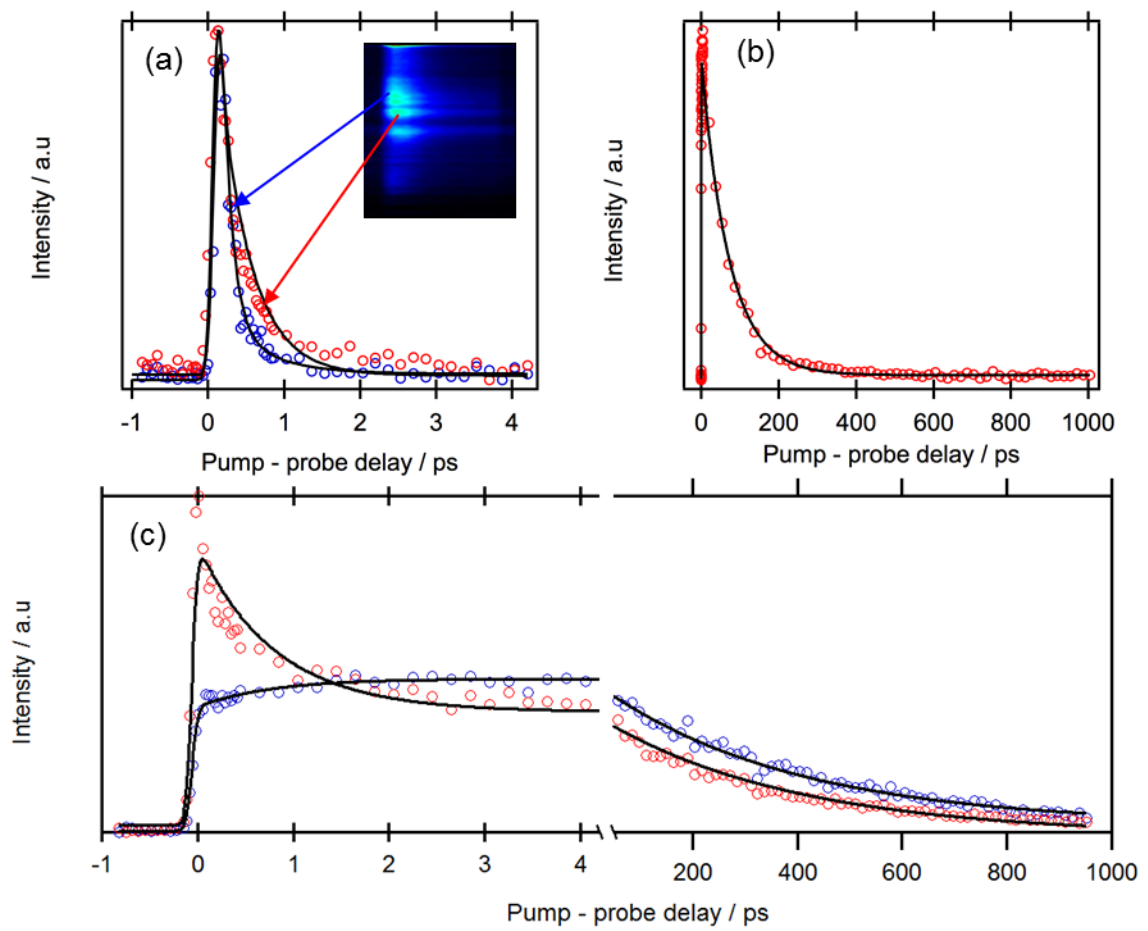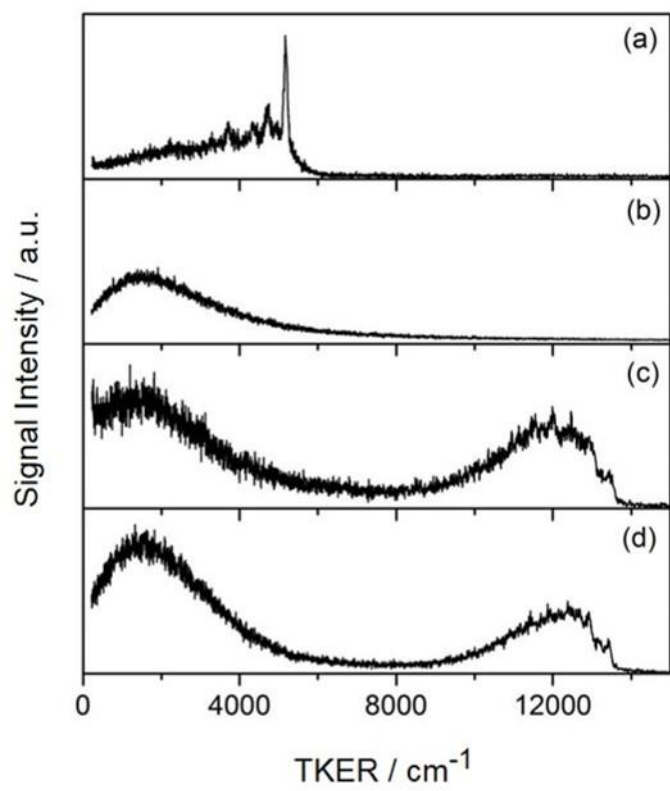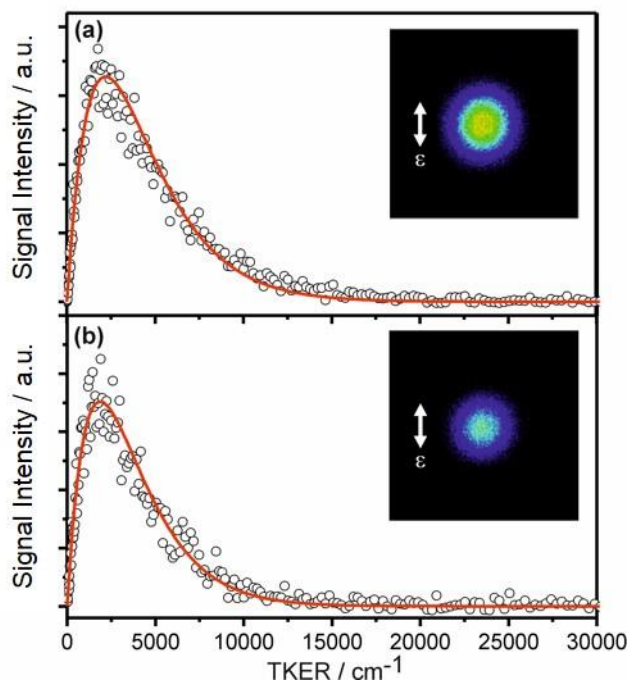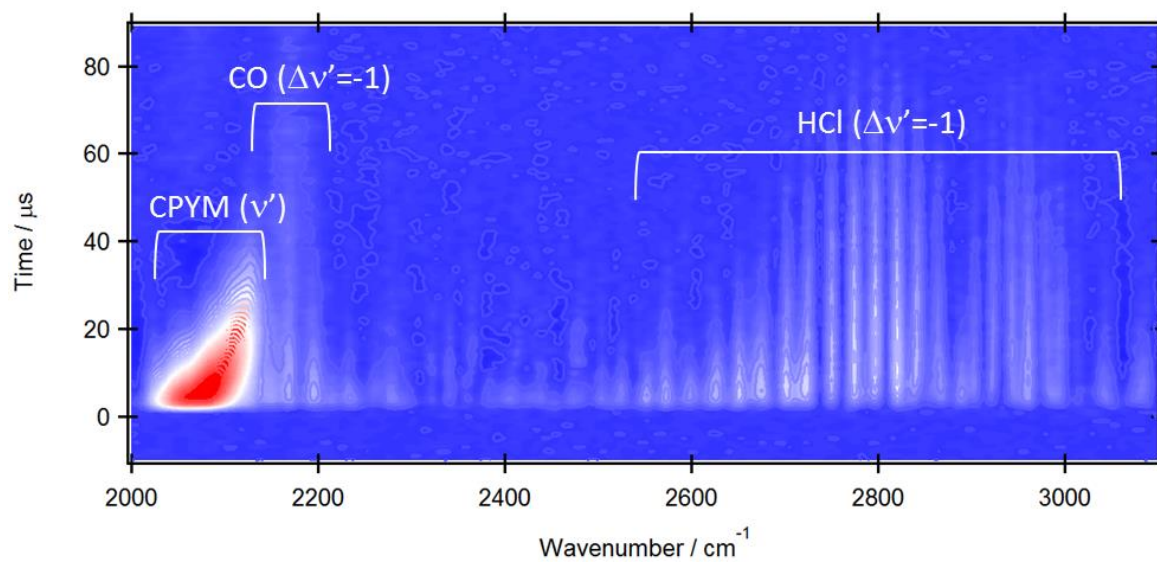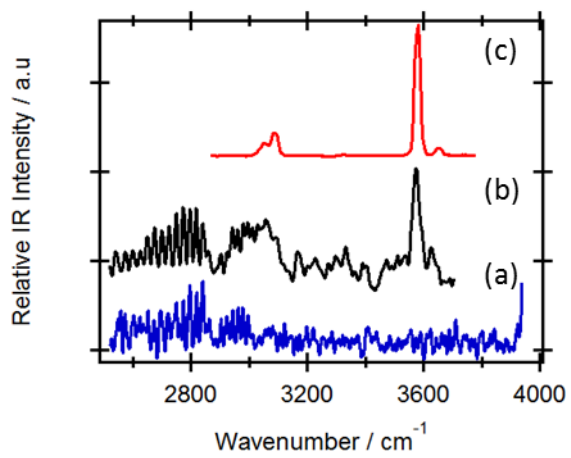
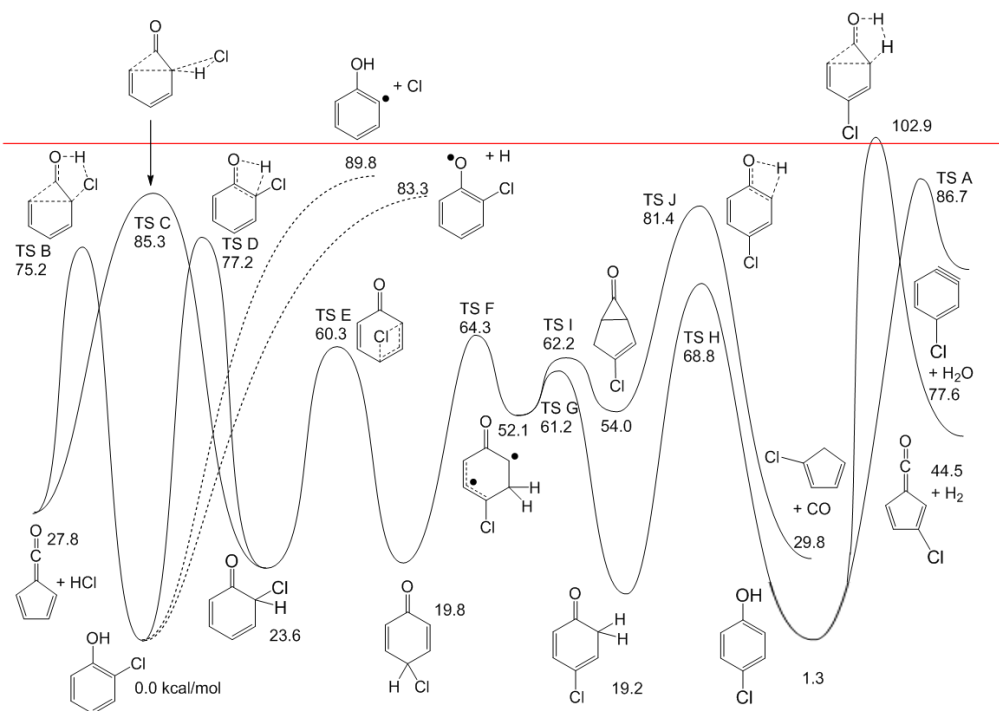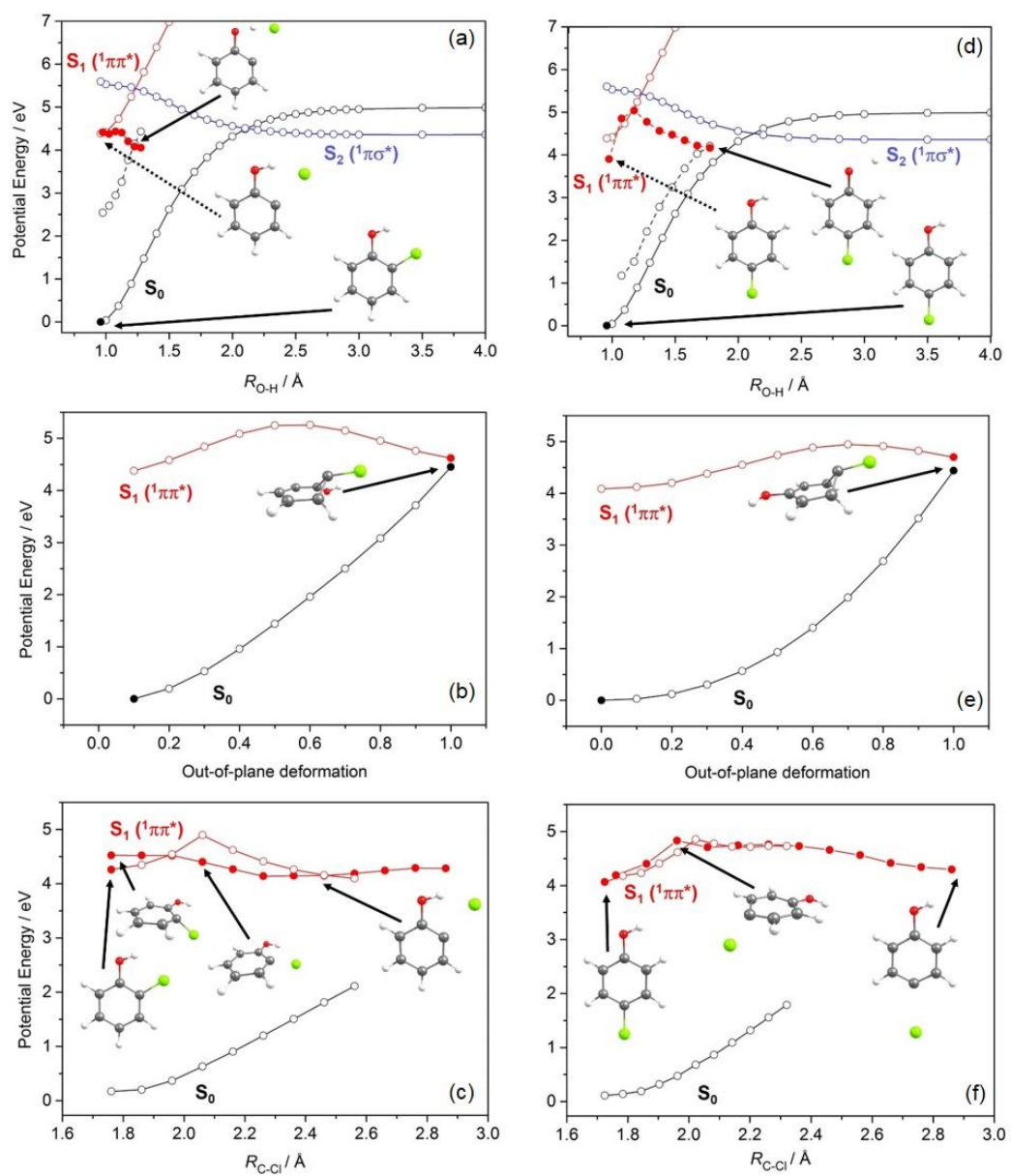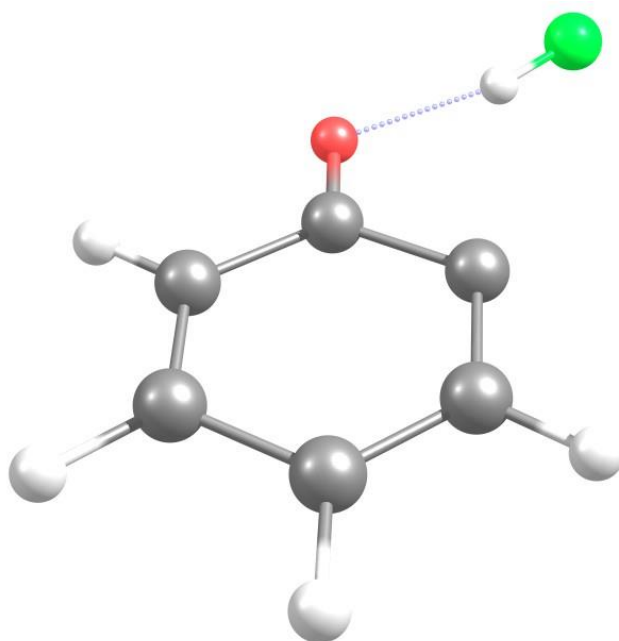**Figure 5**

Figure 6

Figure 7

Figure 8

Figure 9

Figure 10

References

(1)   Tseng, C.-M.; Lee, Y. T.; Ni, C.-K. H Atom Elimination from the πσ* State in the

        Photodissociation of Phenol. *J. Chem. Phys.* **2004**, *121*, 2459–2461.

(2)   Nix, M. G. D.; Devine, A. L.; Cronin, B.; Dixon, R. N.; Ashfold, M. N. R. High

        Resolution Photofragment Translational Spectroscopy Studies of the near Ultraviolet

        Photolysis of Phenol. *J. Chem. Phys.* **2006**, *125*, 133318 – 133331.

(3)   Sobolewski, A. L.; Domcke, W.; Dedonder-Lardeux, C.; Jouvet, C. Excited-State

        Hydrogen Detachment and Hydrogen Transfer Driven by Repulsive ^{1}πσ* States: A

        New Paradigm for Nonradiative Decay in Aromatic Biomolecules. *Phys. Chem. Chem.*

        Phys. **2002**, *4*, 1093–1100.

(4)   Dixon, R. N.; Oliver, T. A. A.; Ashfold, M. N. R. Tunnelling under a Conical

        Intersection: Application to the Product Vibrational State Distributions in the UV

        Photodissociation of Phenols. *J. Chem. Phys.* **2011**, *134*, 194303 – 194313.

(5)   Pino, G. A.; Oldani, A. N.; Marceca, E.; Fujii, M.; Ishiuchi, S.-I.; Miyazaki, M.;

        Broquier, M.; Dedonder, C.; Jouvet, C. Excited State Hydrogen Transfer Dynamics in

        Substituted Phenols and Their Complexes with Ammonia: ππ*-πσ* Energy Gap

        Propensity and Ortho-Substitution Effect. *J. Chem. Phys.* **2010**, *133*, 124313–124325.

(6)   Karsili, T. N. V.; Wenge, A. M.; Harris, S. J.; Murdock, D.; Harvey, J. N.; Dixon, R.

        N.; Ashfold, M. N. R. O–H Bond Fission in 4-Substituted Phenols: S_1 State

        Predissociation Viewed in a Hammett-like Framework. *Chem. Sci.* **2013**, *4*, 2434 –

        2446.

(7)   Karsili, T. N. V; Wenge, A. M.; Marchetti, B.; Ashfold, M. N. R. Symmetry Matters: Photodissociation Dynamics of Symmetrically versus Asymmetrically Substituted Phenols. *Phys. Chem. Chem. Phys.* **2014**, *16*, 588–598.

(8)   Tseng, C.-M.; Lee, Y. T.; Lin, M.-F.; Ni, C.-K.; Liu, S.-Y.; Lee, Y.-P.; Xu, Z. F.; Lin, M. C. Photodissociation Dynamics of Phenol. *J. Phys. Chem. A* **2007**, *111*, 9463–9470.

(9)   Imhof, P.; Kleinermanns, K. Dispersed Fluorescence Spectra of p-Chlorophenol. *Phys. Chem. Chem. Phys.* **2002**, *4*, 264–270.

(10)   Huang, J.; Lin, J. L.; Tzeng, W. B. Mass Analyzed Threshold Ionization Spectroscopy of the ^{35}Cl and ^{37}Cl Isotopomers of P-Chlorophenol and Isotope Effect. *Chem. Phys. Lett.* **2006**, *422*, 271–275.

(11)   Devine, A. L.; Nix, M. G. D.; Cronin, B.; Ashfold, M. N. R. Near-UV Photolysis of Substituted Phenols, I: 4-Fluoro-, 4-Chloro- and 4-Bromophenol. *Phys. Chem. Chem. Phys.* **2007**, *9*, 3749–3762.

(12)   Oikawa, A.; Abe, H.; Mikami, N.; Ito, M. Rotational Isomers of Meta-Substituted Phenols and Beta-Naphthol Studied by Electronic Spectra in Supersonic Free Jets. *J. Phys. Chem.* **1984**, *88*, 5180–5186.

(13)   Yamamoto, S.; Ebata, T.; Ito, M. Rotational Isomers of o-Chlorophenol and Their Different Emission Properties. *J. Phys. Chem.* **1989**, *93*, 6340–6345.

(14)   Oikawa, A.; Abe, H.; Mikami, N.; Ito, M. Electronic Spectra and Ionisation Potentials of Rotational Isomers of Several Disubstituted Benzenes. *Chem. Phys. Lett.* **1985**, *116*, 50–54.

(15) Cockett, M. C. R.; Takahashi, M.; Okuyama, K.; Kimura, K. REMPI Threshold Photoelectron Spectra of the Cis and Trans Rotational Isomers of Jet-Cooled M-Chlorophenol. *Chem. Phys. Lett.* **1991**, *187*, 250–256.

(16) Nakagawa, S.; Matsushita, Y.; Suzuki, T.; Ichimura, T. Resonance Enhanced Multiphoton Ionization and Time-of-Flight Mass Spectra of Jet-Cooled 3-Chlorophenol Dimer. *J. Mol. Struct.* **2005**, *779*, 68–71.

(17) Böhm, M.; Ratzer, C.; Schmitt, M. The Structure of p-Chlorophenol and Barrier to Internal OH Rotation in the S_1-State. *J. Mol. Struct.* **2006**, *800*, 55–61.

(18) Rayne, S.; Forest, K.; Friesen, K. J. Mechanistic Aspects Regarding the Direct Aqueous Environmental Photochemistry of Phenol and Its Simple Halogenated Derivatives. A Review. *Environ. Int.* **2009**, *35*, 425 – 437.

(19) Akai, N.; Kudoh, S.; Takayanagi, M.; Nakata, M. Photoreaction Mechanisms of 2-Chlorophenol and Its Multiple Chloro-Substituted Derivatives Studied by Low-Temperature Matrix-Isolation Infrared Spectroscopy and Density-Functional-Theory Calculations. *Photochem. Photobiol.* **2001**, *146*, 49–57.

(20) Sobolewski, A. L.; Domcke, W. Photophysics of Intramolecularly Hydrogen-Bonded Aromatic Systems: Ab Initio Exploration of the Excited-State Deactivation Mechanisms of Salicylic Acid. *Phys. Chem. Chem. Phys.* **2006**, *8*, 3410–3417.

(21) Yang, Y. L.; Dyakov, Y.; Lee, Y. T.; Ni, C.-K.; Sun, Y.-L.; Hu, W.-P. Photodissociation Dynamics of Hydroxybenzoic Acids. *J. Chem. Phys.* **2011**, *134*, 034314 – 9.

(22)   Sage, A. G.; Oliver, T. A. A.; King, G. A.; Murdock, D.; Harvey, J. N.; Ashfold, M. N. R. UV Photolysis of 4-Iodo-, 4-Bromo-, and 4-Chlorophenol: Competition between C-Y (Y = Halogen) and O-H Bond Fission. *J. Chem. Phys.* **2013**, *138*, 164318 − 164330.

(23)   Wells, K. L.; Perriam, G.; Stavros, V. G. Time-Resolved Velocity Map Ion Imaging Study of NH_3 Photodissociation. *J. Chem. Phys.* **2009**, *130*, 074308 − 074313.

(24)   Hancock, G.; Heard, D. E. Time-Resolved FTIR Emission Studies of Photochemical Reactions. *Adv. Photochem.* **1993**, *18*, 1−65.

(25)   Hancock, G.; Morrison, M.; Saunders, M. Vibrational Relaxation of NO (v = 1-16) with NO, N_2O, NO_2, He and Ar Studied by Time-Resolved Fourier Transform Infrared Emission. *Phys. Chem. Chem. Phys.* **2009**, *11*, 8507−8515.

(26)   Poisson, L.; Nandi, D.; Soep, B.; Hochlaf, M.; Boggio-Pasqua, M.; Mestdagh, J.-M. A Roaming Wavepacket in the Dynamics of Electronically Excited 2-Hydroxypyridine. *Phys. Chem. Chem. Phys.* **2014**, *16*, 581−587.

(27)   Spighi, G.; Gaveau, M.-A.; Mestdagh, J.-M.; Poisson, L.; Soep, B. Gas Phase Dynamics of Triplet Formation in Benzophenone. *Phys. Chem. Chem. Phys.* **2014**, *16*, 9610−9618.

(28)   Tseplin, E. E.; Tseplina, S. N.; Tuimedov, G. M.; Khvostenko, O. G. Identification of Excited Singlet States of Chlorophenol Isomers. *Opt. Spectrosc.* **2008**, *105*, 327−332.

(29)   Tseplin, E. E.; Tseplina, S. N.; Tuimedov, G. M.; Khvostenko, O. G. Photoelectron and UV Absorption Spectroscopy for Determination of Electronic Configurations of Negative Molecular Ions: Chlorophenols. *J. Electron Spectros. Relat. Phenomena* **2009**, *171*, 37−46.

(30)   Roberts, G. M.; Chatterley, A. S.; Young, J. D.; Stavros, V. G. Direct Observation of Hydrogen Tunneling Dynamics in Photoexcited Phenol. *J. Phys. Chem. Lett.* **2012**, *3*, 348–352.

(31)   Remmers, K.; Meerts, W. L.; Zehnacker-Rentien, A.; Le Barbu, K.; Lahmani, F. Structural Information on the S_0 and S_1 State of O-Fluorophenol by Hole Burning and High Resolution Ultraviolet Spectroscopy. *J. Chem. Phys.* **2000**, *112*, 6237 – 6244.

(32)   Schick, C. P.; Weber, P. M. Ultrafast Dynamics in Superexcited States of Phenol. *J. Phys. Chem. A* **2001**, *105*, 3725–3734.

(33)   Arepalli, S.; Presser, N.; Gordon, R. J. Detection of Cl Atoms and HCl Molecules by Resonantly Enhanced Multiphoton Ionisation. *Chem. Phys. Lett.* **1985**, *118*, 88–92.

(34)   Shin, D. N.; Hahn, J. W.; Jung, K.; Ha, T. Study of the Cis and Trans Conformers of 2-Halophenols Using Coherent Anti-Stokes Raman Spectroscopic and Quantum Chemical Methods. *Chem. Phys. Lett.* **1998**, *29*, 245–249.

(35)   Nagaoka, S.; Takemura, T.; Baba, H.; Koga, N.; Morokuma, K. Ab Initio Study on the Low-Lying Triplet States of Chlorobenzene. *J. Phys. Chem.* **1986**, *90*, 759–763.

(36)   Xu, Z. F.; Lin, M. C. Ab Initio Kinetics for the Unimolecular Reaction C_6H_5OH --> CO + C5H6. *J. Phys. Chem. A* **2006**, *110*, 1672–1677.

(37)   Altarawneh, M.; Dlugogorski, B. Z.; Kennedy, E. M.; Mackie, J. C. Quantum Chemical and Kinetic Study of Formation of 2-Chlorophenoxy Radical from 2-Chlorophenol: Unimolecular Decomposition and Bimolecular Reactions with H, OH, Cl, and O_2. *J. Phys. Chem. A* **2008**, *112*, 3680–3692.

(38)   Le, H. T.; Flammang, R.; Gerbaux, P.; Bouchoux, G.; Nguyen, M. T. Ionized Phenol

and Its Isomers in the Gas Phase. *J. Phys. Chem.* **2001**, *105*, 11582–11592.

(39)   Lasorne, B.; Bearpark, M. J.; Robb, M. A.; Worth, G. A. Controlling S_1 / S_0 Decay and

the Balance between Photochemistry and Photostability in Benzene : A Direct

Quantum Dynamics Study. *J. Phys. Chem. A* **2008**, *112*, 13017–13027.

(40)   Ratzer, C.; Nispel, M.; Schmitt, M. Structure of 4-Fluorophenol and Barrier to Internal

−OH Rotation in the S1-State. *Phys. Chem. Chem. Phys.* **2003**, *5*, 812–819.

(41)   Spangenberg, D.; Schmitt, M.; Ratzer, C.; Jochen, K. The Structure of Phenol in the S_1

-State Determined by High Resolution UV-Spectroscopy. *Chem. Phys.* **2002**, *283*,

153–169.